JOURNAL OF SPACECRAFT AND ROCKETS
Vol. 32, No. 2, March–April 1995

Modeling of Ionizing Hypersonic Flows in Nonequilibrium

F. Grasso* and G. Capano†
University of Rome "La Sapienza," 18-00184 Rome, Italy

A two-temperature model is developed for the description of thermal and chemical nonequilibrium viscous hypersonic flows including ionization. A preferential dissociation model and nonpreferential removal of vibrational and electronic energy are assumed. For weakly ionized flows, an ambipolar diffusion coefficient is introduced to describe ion diffusion. The numerical technique relies on a finite-volume approach based on a second-order accurate Total-Variation-Diminishing formulation that allows for thermal and chemical nonequilibrium effects as well as for ionization. The model has been applied to compute ionizing hypersonic flows over a wedge and a RAM-C geometry. Applications have shown that, for weakly ionized flows, ionization is essentially decoupled from the other field properties. Moreover, the computations show the importance of considering kinetic and diffusive mechanisms fully coupled in order to properly understand the flow features.

Nomenclature

a = eigenvalue of inviscid-flux Jacobian
$\mathbf{b}$ = span base vector
c = frozen speed of sound
c_v = constant-volume specific heat
D = diffusion coefficient
E = total energy; activation energy
e = internal energy; electron charge
e^- = free electron
$\mathbf{F}$ = sum of inviscid and viscous fluxes; x component of flux
$\mathbf{G}$ = y component of flux
$\mathbf{H}$ = source-term vector
H = total enthalpy
h = enthalpy
K = pressure derivatives
k = Boltzmann constant
m = mass of molecule
$\mathbf{n}$ = outward unit normal
n = number density
p = pressure
$\mathbf{Q}$ = total heat flux
$\mathbf{R}$ = right eigenvector matrix
R = gas constant
S = cell area; thermal-nonequilibrium source term
T = temperature
u,v = velocity components
$\mathbf{V}$ = diffusion velocity
$\mathbf{W}$ = vector unknown
W = molecular weight
w = chemical nonequilibrium source term
X = molar fraction
x, y = coordinates
Y = mass fraction
α = difference of characteristic variables
β = cell face
δ_{sq} = Kronecker delta
Δ = collision integral
Δh° = enthalpy of formation
Δs = cell face length
ϵ = energy per unit volume
η = thermal conductivity
θ = characteristic temperature
μ = viscosity
ν^* = effective collision frequency
ρ = density
σ = total stress tensor; collision cross section
τ = vibrational relaxation time
χ = pressure derivative

Subscripts

E = inviscid contribution; electronic
Ec = electronic excitation
el = free electron
e = electronic; electron
I = ion
i, j = cell indices
num = numerical
p, q = pth, qth species
R = removal
rot = rotational
T = translational
tr = translational
V = viscous contribution; vibrational-electron-electronic
v = vibrational
x, y = x, y components
∞ = freestream

Superscripts

e = electronic
ℓ = ℓth component
q = qth species
v = vibrational
$+$ = ion
$'$ = heavy particle

Received Dec. 20, 1993; revision received May 27, 1994; accepted for publication May 31, 1994.

*Associate Professor, Department of Mechanics and Aeronautics, Via Eudossiana. Member AIAA.

†Graduate Student, Department of Mechanics and Aeronautics, Via Eudossiana.

Introduction

TO develop an advanced space transportation systems at high speeds, the high-temperature effects must be understood in detail. In the flows through bow shocks or within the boundary layer, the high kinetic energy content is converted in internal energy, thus increasing the (translational) temperature of the gas. The high temperature causes vibrational and electronic excitation, dissociation of diatomic molecules, and ionization. Under typical hypersonic conditions, air must be considered as a mixture of reacting gases whose thermodynamic state is characterized by: 1) a translational

temperature (identifying the translational and rotational energy modes), 2) a vibrational temperature for each of the polyatomic species (identifying the vibrational energy contribution), and 3) an electronic temperature (for the electronic energy contribution of the heavy particles and for the translational contribution of the free electrons).

Depending upon the characteristic scales of the exchange processes, different chemical states may arise, i.e., equilibrium, frozen, and nonequilibrium. In the present work, we focus our attention on flows characterized by finite-rate processes, i.e. by nonequilibrium processes with ionization. The simulation of thermal- and chemical-nonequilibrium hypersonic flows with ionization has been investigated by several authors. Deiwert and Candler[1] assume 1) rapid energy exchange between the translational and rotational modes, 2) a finite energy transfer rate for the vibrational modes of the different diatomic species, and 3) the same temperature characterizing electron translation and electronic modes. For the coupling between vibration and dissociation Deiwert and Candler assume a nonpreferential removal of vibrational energy. For high-temperature ionized air Deiwert and Candler developed a six-temperature model to compute Aeroassist Orbit Transfer Vehicle (AOTV) flight experiments, and have shown the influence of thermochemical nonequilibrium on the flowfield. Palmer[2] has developed a two-temperature model to compute dissociating, ionizing flows in thermochemical nonequilibrium. He also assumes a simple model for vibration-dissociation coupling as proposed by Deiwert and Candler. Applications of the model to compute flows such as those in the Aeroassist Flight Experiment (AFE) and Radio Attenuation Measurement Experiment (RAM-C) show reasonably accurate solutions. Hatfield and Candler[3] have used a three-temperature model to study nonequilibrium effects in a one-dimensional ionized-nitrogen flow, and have developed a technique to remove some inconsistencies encountered in the treatment of the electron pressure contribution as originally proposed in Ref. 1. Mitcheltree[4] has investigated the application of several dissociation and ionization models for high-velocity entries with a two-temperature model, where the chemical-vibrational coupling is taken into account by means of a weighted dissociation rate controlling the temperature. Gnoffo et al.[5] have developed a rather complete model for thermal- and chemical-nonequilibrium ionizing flows based on either a two- or a three-temperature model. Those authors assume curve fits for the thermodynamic relations and collision integrals, and a preferential dissociation model similar to that of Ref. 1. Applications of the model to compute AFE flows show limitations arising from uncertainties in the thermodynamic and collision-integral curve fits, the chemical reaction mechanism, and the effects of preferential dissociation modeling. In the absence of ionization, Grasso and Bellucci[6] have developed a two-temperature model for thermochemical-nonequilibrium flows, which employs a vibrational coupling factor and a nonpreferential removal of vibrational energy. Applications of the model have shown the influence of thermal nonequilibrium on the properties of the flowfield.

It must be pointed out that most of the nonequilibrium hypersonic flow simulations with ionization consider the flow weakly ionized, and plasmadynamic effects are generally neglected. This is believed to be a good approximation for many forebody flowfields of aerospace interest. However, Shebalin[7] has recently shown that macroscopic plasmadynamics may affect the flow past an ionizing bowshock around an aerobraking spacecraft.

In the present paper we develop a model for thermochemical-nonequilibrium flows, with ionization, under the assumption of a rapid energy exchange between the vibrational and electron-electronic modes and weak ionization. The diffusional effects on the translational-vibrational energy exchanges are neglected, perfect-gas relations are used to determine the thermodynamic relations, and collision-integral curve fits are employed for the transport mechanism. Moreover, expressions derived from classical kinetic theory are used to evaluate the energy exchanges between translational modes of electrons and heavy particles. The equations are solved by a finite-volume approach based on a total-variation-diminishing scheme that allows for nonequilibrium effects and ionization. The model has been applied to compute ionizing nonequilibrium flows over a wedge and over a RAM-C geometry (blunt 9-deg cone).

Governing Equations

The governing equations are the conservation equations for a mixture of gases in thermal and chemical nonequilibrium under the continuum assumption. The model assumes a single translational temperature (T, which characterizes the translational modes and the fully excited rotational modes) and a single vibrational-electron-electronic temperature (T_V, which characterizes the vibrational and electronic modes of heavy particles and the translational modes of the free electrons). Moreover, neglecting externally applied electric and magnetic fields, it is assumed that charge separation and conduction currents are negligible. In vector form the conservation equations are

$$\frac{\partial}{\partial t}\int_S \mathbf{W}\,dS + \oint_{\partial S} \mathbf{F}\cdot\mathbf{n}\,ds = \int_S \mathbf{H}\,dS \tag{1}$$

where

$$\mathbf{W} = [\rho_q, \rho u, \rho v, \rho E, \rho e_V]^T$$

$$\mathbf{F} = (\mathbf{F}_E - \mathbf{F}_V, \mathbf{G}_E - \mathbf{G}_V)$$

$$\mathbf{H} = [w_q, 0, 0, 0, S_V]^T$$

$$\mathbf{F}_E = \left[\rho_q u, \rho u^2 + p, \rho uv, \rho uH, \rho u e_V\right]^T$$

$$\mathbf{G}_E = \left[\rho_q v, \rho uv, \rho v^2 + p, \rho vH, \rho v e_V\right]^T$$

$$(\mathbf{F}_V, \mathbf{G}_V) = [-\rho_q \mathbf{V}_q, \boldsymbol{\sigma}, \mathbf{u}\cdot\boldsymbol{\sigma} - \mathbf{Q}, -\mathbf{Q}_V]^T$$

and

$$\boldsymbol{\sigma} = \mu\left[\nabla\mathbf{u} + (\nabla\mathbf{u})^T\right] - \tfrac{2}{3}\mu(\nabla\cdot\mathbf{u})\mathbf{I}$$

$$\mathbf{Q} = -(\eta_{tr} + \eta_{rot})\nabla T$$

$$-(\eta_v + \eta_{Ec} + \eta_{el})\nabla T_V + \sum_q h_q \rho_q \mathbf{V}_q$$

$$\mathbf{Q}_V = -(\eta_v + \eta_{Ec} + \eta_{el})\nabla T_V + \sum_q h_V^q \rho_q \mathbf{V}_q$$

$$E = \sum_q Y_q e_q + \frac{u^2 + v^2}{2}$$

$$H = E + \frac{p}{\rho}$$

$$\rho = \sum_q \rho_q$$

$$\rho_q \mathbf{V}_q = -\rho D_q \nabla X_q$$

For heavy particles, $h_V^q = e_V^q$, while for electrons $h_{el} = h_V^e = e_{el} + p_e/\rho_e$, and the vibrational-electron-electronic energy source term is

$$S_V = -p_e \nabla\cdot\mathbf{u} + S_{T\text{-}V} + S_{T\text{-}E} + S_{E\text{-}R}$$

(note that S_V includes the term $-p_e\nabla\cdot\mathbf{u}$, which is the electron pressure work and is related to the work of the electric field).

Thermodynamic Relations

In general the internal energy and the enthalpy of species q are functions of the translational and vibrational temperatures. Assuming mode separability, the internal energy of the heavy species is the sum of the translational and internal contributions.[8,9]

For atomic species, one has

$$e_q = \tfrac{3}{2}R_q T + e_E^q + \Delta h_q^\circ \tag{2}$$

For diatomic species, assuming full excitation of the rotational modes, one obtains

$$e_q = \tfrac{5}{2} R_q T + e_{\mathrm{v}}^q + e_{\mathrm{E}}^q + \Delta h_q^\circ \tag{3}$$

The electron translational energy is given by

$$e_{\mathrm{el}} = \tfrac{3}{2} R_{\mathrm{e}} T_{\mathrm{V}} \tag{4}$$

The vibrational and electronic energy contributions are obtained assuming Boltzmann distributions at the vibrational-electron-electronic temperature T_{V}, thus yielding

$$e_{\mathrm{v}}^q = R_q \theta_q^{\mathrm{v}} \frac{1}{\exp\left(\theta_q^{\mathrm{v}}/T_{\mathrm{v}}\right) - 1} \tag{5}$$

$$e_{\mathrm{E}}^q = R_q \frac{\sum_{i=1}^{N_q^{\mathrm{e}}} g_{q,i} \theta_{q,i}^{\mathrm{e}} \exp\left(-\theta_{q,i}^{\mathrm{e}}/T_{\mathrm{V}}\right)}{\sum_{i=1}^{N_q^{\mathrm{e}}} g_{q,i} \exp\left(-\theta_{q,i}^{\mathrm{e}}/T_{\mathrm{V}}\right)} \tag{6}$$

where $g_{q,i}$ represents the ith-state degeneracy.[8–10]

Because of vibration-dissociation coupling, dissociation occurs mainly at the higher vibrational levels. For harmonic oscillator behavior, only a finite number of such levels can then be taken into account in evaluating the vibrational energy.[9] The number of vibrational levels before the occurrence of dissociation depends on the dissociation energy of each molecule. For nitric oxide, molecular oxygen, molecular nitrogen, and nitric oxide ions one obtains $N_{\mathrm{NO}}^{\mathrm{v}} = 28$, $N_{\mathrm{O_2}}^{\mathrm{v}} = 27$, $N_{\mathrm{N_2}}^{\mathrm{v}} = 34$, $N_{\mathrm{NO^+}}^{\mathrm{v}} = 37$.

In the present work, it has been assumed that associative ionization of atomic nitrogen and oxygen is mainly responsible for the production of nitric oxide ions (NO^+) and electrons (as discussed in a later section). For the six heavy species that have been considered [O, N, NO, O_2, N_2, NO^+], the number of electronic states given in Ref. 10 is $N_q^{\mathrm{e}} = 19, 22, 15, 19, 11, 8$. However, spectroscopic data for the higher electronic states are uncertain; moreover, if the temperature is below 10,000 K, a reduced number of electronic states can be used. Park and Yoon[11] argue that the only excited electronic states are those that have an energy exceeding that of the ground state by less than 2 eV, thus obtaining $N_q^{\mathrm{e}} = 2, 2, 0, 3, 0, 0$. Likewise, in Ref. 2 the electronic excitation of nitric oxide, diatomic nitrogen, and nitric oxide ions is neglected, and $N_q^{\mathrm{e}} = 3, 3, 0, 3, 0, 0$, whereas Ref. 1 uses the first two levels for all species. In the present model the number of electronic states has been determined by requiring that the percentage error of the internal energy of each species, computed with a reduced number of states, be less than 1% of the value obtained by allowing for all electronic states, which gives $N_q^{\mathrm{e}} = 2, 3, 2, 7, 2, 1$.

Transport Coefficients

At high temperature the transport properties (viscosity, thermal conductivity, and diffusion coefficients) are affected by chemical composition, besides the translational and vibrational-electron-electronic temperature dependencies.

In the present work the transport coefficients are based on the Chapman-Enskog theory, extended to include the effects of momentum and energy transfer between different species by collisions.[12] This is done by introducing the collision integrals ($\Delta_{q,r}^{(k)}$, $k = 1, 2$), which depend upon the dynamics of the collisions between particle of types q and r, and on the interaction energy potential. Following the work of Refs. 5, 12, and 13, the collision integrals for encounter of heavy particles with each other are evaluated at the heavy-particle translational temperature T, while those for collisions between electrons and any other particle are evaluated at the electron temperature T_{V}.

The mixture viscosity is defined as

$$\mu = \sum_{q=1}^{N-1} \frac{m_q \gamma_q}{\sum_{r \neq e} \gamma_r \Delta_{q,r}^{(2)}(T) + \gamma_e \Delta_{q,e}^{(2)}(T_{\mathrm{V}})} + \frac{m_e \gamma_e}{\sum_{r=1}^{N} \gamma_r \Delta_{e,r}^{(2)}(T_{\mathrm{V}})} \tag{7}$$

where $\gamma_q = Y_q / W_q$ is the molar concentration.

For a mixture of gases in thermal nonequilibrium, the heat conduction include the contributions of the different energy modes.

The translational thermal conductivity of the heavy particles is defined as

$$\eta_{\mathrm{tr}} = \frac{15}{4} k \sum_{q=1}^{N-1} \frac{\gamma_q}{\sum_{r \neq e} a_{q,r} \gamma_r \Delta_{q,r}^{(2)}(T) + 3.54 \gamma_e \Delta_{q,e}^{(2)}(T_{\mathrm{V}})} \tag{8}$$

with

$$a_{q,r} = 1 + \frac{[1 - (m_q/m_r)][0.45 - 2.54(m_q/m_r)]}{[1 + (m_q/m_r)]^2} \tag{9}$$

For the fully excited rotational mode we have

$$\eta_{\mathrm{rot}} = k \sum_{q\ \mathrm{mol}} \frac{\gamma_q}{\sum_{r \neq e} \gamma_r \Delta_{q,r}^{(1)}(T) + \gamma_e \Delta_{q,e}^{(1)}(T_{\mathrm{V}})} \tag{10}$$

where the q summation is over all diatomic species.

For the vibrational and electronic thermal conductivity we have used a simplified expression corresponding to partial excitation of the two modes, thus obtaining

$$\eta_{\mathrm{v}} = k \sum_{q\ \mathrm{mol}} \frac{\gamma_q \left(c_{\mathrm{vv}}^q / R_q\right)}{\sum_{r \neq e} \gamma_r \Delta_{q,r}^{(1)}(T) + \gamma_e \Delta_{q,e}^{(1)}(T_{\mathrm{V}})} \tag{11}$$

$$\eta_{\mathrm{Ec}} = k \sum_{q=1}^{N-1} \frac{\gamma_q \left(c_{\mathrm{vE}}^q / R_q\right)}{\sum_{r \neq e} \gamma_r \Delta_{q,r}^{(1)}(T) + \gamma_e \Delta_{q,e}^{(1)}(T_{\mathrm{V}})} \tag{12}$$

The free-electron translational thermal conductivity is expressed as

$$\eta_{\mathrm{el}} = \frac{15}{4} k \frac{\gamma_e}{\sum_{r \neq e} 1.45 \gamma_r \Delta_{e,r}^{(2)}(T_{\mathrm{V}}) + \gamma_e \Delta_{e,e}^{(2)}(T_{\mathrm{V}})} \tag{13}$$

The diffusion coefficient of species q in the mixture is given by

$$D_q = \frac{k T}{p} \frac{\gamma_t^2 W_q (1 - W_q \gamma_q)}{\sum_{r \neq q} \gamma_r \Delta_{q,r}^{(1)}} \tag{14}$$

where $\gamma_t = \sum_q \gamma_q$.

In a partially ionized gas, with the assumptions of zero electric current and charge neutrality, the induced electric field affects the diffusion of the charged species. As shown in Refs. 5 and 13, the effective diffusion coefficient of the electrons (D_e) is proportional to the ambipolar diffusion coefficient of the ions, i.e.,

$$D_e = \frac{m_e}{m_{\mathrm{NO^+}}} D_{\mathrm{NO^+}}^{\mathrm{amb}} = \frac{m_e}{m_{\mathrm{NO^+}}} 2 D_{\mathrm{NO^+}} \tag{15}$$

Chemistry Model

Finite-rate chemistry has been modeled by using the 17-reaction mechanism of Ref. 10. Moreover, for weak ionization we have only considered the least endothermic associative ionization reaction, thus obtaining

$$\begin{aligned} \mathrm{O_2} + M &\leftrightarrows \mathrm{O} + \mathrm{O} + M \\ \mathrm{NO} + M &\leftrightarrows \mathrm{N} + \mathrm{O} + M \\ \mathrm{N_2} + M &\leftrightarrows \mathrm{N} + \mathrm{N} + M \\ \mathrm{N_2} + \mathrm{O} &\leftrightarrows \mathrm{NO} + \mathrm{N} \\ \mathrm{NO} + \mathrm{O} &\leftrightarrows \mathrm{O_2} + \mathrm{N} \\ \mathrm{N} + \mathrm{O} &\leftrightarrows \mathrm{NO^+} + e^- \end{aligned} \tag{16}$$

where M is any of the neutral species. The forward and backward reaction rate constants are evaluated as

$$k_{\mathrm{f},r} = C_{\mathrm{f},r} T_{\mathrm{d}}^{\eta_{\mathrm{f},r}} \exp(-E_{\mathrm{f},r}/kT_{\mathrm{d}}) \tag{17}$$

$$k_{\mathrm{b},r} = \frac{k_{\mathrm{f},r}}{k_{\mathrm{eq},r}} \tag{18}$$

where the equilibrium constant $k_{eq,r}$ is defined in Ref. 14, the constants C and η are, respectively, the Arrhenius constants and the pre-exponential factors (given in Ref. 10); the reaction-rate-controlling temperature of the dissociation reactions, which reflects the coupling between vibration and dissociation, is defined as

$$T_d = T^n\, T_V^{1-n}$$

In Ref. 5 a value of $n = 0.5$ was found to place too much weight on T_V. More recently Park[10] and the authors of Ref. 5 used a value of $n = 0.7$, thus obtaining faster dissociation reactions immediately past the shock. References 4 and 15 introduced a dependence of n upon the vibrational temperature. In the present work we have chosen[16] the value $n = 0.5$; moreover, for the dissociative ionic recombination, which is characterized by electron translational modes and vibrational energy modes of ions, we have followed the approach of Ref. 1 and have assumed $T_d = T_V$.

Vibrational-Electron-Electronic Energy Exchanges

Referring to the vibrational-electron-electronic equation, the source term S_V includes the translational-vibrational energy exchanges ($S_{T\text{-}V}$), the heavy-particle–electron translational energy exchanges ($S_{T\text{-}E}$), and the vibrational-electron-electronic energy lost (or gained) in chemical reactions ($S_{E\text{-}R}$).

The T-V energy exchanges are modeled according to Landau-Teller theory[8–10]:

$$S_{T\text{-}V} = \sum_{q\ \mathrm{mol}} \rho_q \frac{e_V^q(T) - e_V^q(T_V)}{\tau_q} \tag{19}$$

where[10] the vibrational relaxation time is defined as the sum of the molar averaged Millikan-White[17] relaxation time $\tau_q^{M\text{-}W}$ and the collision-limited[10] time τ_q^P:

$$\tau_q = \tau_q^{M\text{-}W} + \tau_q^P \tag{20}$$

where

$$\tau_q^{M\text{-}W} = \frac{\sum_r X_r}{\sum_r \frac{X_r}{\tau_{qr}}}, \qquad r \neq e \tag{21}$$

$$\tau_{q,r} = \frac{1}{p}\exp\left[A_{q,r}\left(T^{-\frac{1}{3}} - 0.015 W_{qr}^{\frac{1}{4}}\right) - 18.42\right]$$

$$A_{q,r} = 1.16 \times 10^{-3} W_{qr}^{\frac{1}{2}} \theta_q^{v\,\frac{4}{3}}$$

$$\frac{1}{\tau_q^P} = 6.02252 \times 10^2 \left(8\frac{R_q T}{\pi}\right)^{1/2} \left(\frac{50,000}{T}\right)^2 \frac{\rho_q}{W_q}$$

The heavy-particle–electron translational energy exchanges are derived from classical kinetic theory, under the assumption of a displaced Maxwellian distribution function of molecular velocity (i.e., in a frame of reference moving with the mean flow velocity of the species). Neglecting frictional heating of the electrons due to differences between the electron and heavy-particle velocities, one obtains

$$S_{T\text{-}E} = 2 m_e n_e \sum_r \frac{3}{2}\frac{k}{m_r}(T - T_V)\nu_{er}^* \tag{22}$$

where ν_{er}^* is the collision frequency for electrons and species r.

The effective collision frequency for electron-ion and electron–neutral-particle encounters is determined as suggested in Refs. 1 and 18:

$$\nu_{ei}^* = \frac{64}{27}\left(\frac{\pi}{m_e}\right)^{\frac{1}{2}} n_I \frac{e^4}{(2kT_V)^{\frac{3}{2}}} \ln\left[\frac{9}{4}\frac{(kT_V)^3}{\pi n_e e^6}\right] \tag{23}$$

$$\nu_{en}^* = n_n \sigma_{en}\left(\frac{8kT_V}{\pi m_e}\right)^{\frac{1}{2}} \tag{24}$$

where σ_{en} is assumed to be constant over the most likely range of electron temperature T_V and is set equal to $\sigma_{en} = 10^{-16}\mathrm{cm}^2$.

The energy removal contribution due to coupling between chemistry and vibration and to electron-electronic excitations has been assumed to be related to the average vibrational and electron-electronic energies, as also assumed in Refs. 1, 2, and 5, i.e.,

$$S_{E\text{-}R} = w_e e_{el} + \sum_{\mathrm{mol}} w_q e_V^q \tag{25}$$

Numerical Solution

The solution of the governing equations for high-speed flows requires the use of robust and accurate schemes. The flux-difference splitting of Roe in Ref. 19 and the flux-vector splitting of Refs. 20 and 21 have been widely used for (perfect-gas) high-speed flow computations. Roe's approximate Riemann solver has been extended[22] to (real-gas) hypersonic flows in equilibrium. Flux-vector splitting for real gases has been developed in Refs. 3, 23, and 24. A second-order symmetric total-variation-diminishing (TVD) scheme for inviscid flows was implemented in Ref. 25 for chemical equilibrium. A more general methodology for the solution of hypersonic flows in nonequilibrium has been presented in Ref. 26. Grasso and Bellucci have followed the approach of Ref. 26 to develop a second-order method to include thermal- and chemical-nonequilibrium effects.[6] In the present work we have extended the latter two approaches to ionizing nonequilibrium flows.

Space and time discretizations are separated by using the method of lines, and a system of ordinary differential equations is obtained for every computational cell. A cell-centered finite-volume formulation is employed. By approximating surface and boundary integrals by means of the mean-value theorem and midpoint rule, the governing equations are cast in the following discretized form:

$$S_{i,j}\frac{d\mathbf{W}_{i,j}}{dt} + \sum_{\beta=1}^{4}(\mathbf{F}_{num}\cdot\mathbf{n}\,\Delta s)_\beta = S_{i,j}\mathbf{H}_{i,j} \tag{26}$$

The inviscid discretization is based on an upwind biased second-order TVD scheme that includes for nonequilibrium and ionization. The scheme has good properties of monotonicity and conservativity in the presence of discontinuities, and it yields second-order accuracy and oscillation-free solutions. By enforcing consistency at cell face $(i+\frac{1}{2}, j)$, the numerical inviscid-flux discretization is cast in the following form:

$$(\mathbf{F}_{E,num}n_x + \mathbf{G}_{E,num}n_y)_{i+\frac{1}{2},j} = \tfrac{1}{2}\big[(\mathbf{F}_E n_x + \mathbf{G}_E n_y)_{i,j}$$

$$+ (\mathbf{F}_E n_x + \mathbf{G}_E n_y)_{i+1,j} + \mathbf{R}_{i+\frac{1}{2},j}\boldsymbol{\Phi}_{i+\frac{1}{2},j}\big]$$

The expression for the elements of the vector $\boldsymbol{\Phi}_{i+\frac{1}{2},j}$ is obtained by characteristic decomposition in the direction normal to the cell face:

$$\varphi_{i+\frac{1}{2},j}^{\ell} = \tfrac{1}{2}\psi\left(a_{i+\frac{1}{2},j}^{\ell}\right)\left(g_{i+1,j}^{\ell} + g_{i,j}^{\ell}\right)$$

$$- \psi\left(a_{i+1/2,j}^{\ell} + \gamma_{i+1/2,j}^{\ell}\right)\alpha_{i+1/2,j}^{\ell}$$

where

$$\boldsymbol{\alpha}_{i+\frac{1}{2},j} = \mathbf{R}_{i+\frac{1}{2},j}^{-1}(\mathbf{W}_{i+1,j} - \mathbf{W}_{i,j})$$

$$\gamma_{i+\frac{1}{2},j}^{\ell} = \tfrac{1}{2}\psi\left(a_{i+\frac{1}{2},j}^{\ell}\right)\left(g_{i+1,j}^{\ell} - g_{i,j}^{\ell}\right)\Big/\alpha_{i+\frac{1}{2},j}^{\ell}$$

$$g_{i,j}^{\ell} = \mathrm{minmod}\left(\alpha_{i+\frac{1}{2},j}^{\ell}, \alpha_{i-\frac{1}{2},j}^{\ell}\right)$$

$$\mathrm{minmod}(x, y) = \mathrm{sgn}(x)\ \max\{0, \min[|x|, y\,\mathrm{sgn}(x)]\}$$

Here $\psi(z)$ is an entropy correction to $|z|$. The minmod limiter has been used for the second-order antidiffusive flux contribution g,

for its computational efficiency and speed of convergence. Following the work of Vinokur,[26] the right eigenvector matrix is defined as

$$\mathbf{R} = \begin{bmatrix} \delta_{sq} & 0 & 0 & Y_s & Y_s \\ u & -cn_y & 0 & u+cn_x & u-cn_x \\ v & cn_x & 0 & v+cn_y & v-cn_y \\ \mathbf{u}\cdot\mathbf{u}/2-\chi_q/K & c(\mathbf{u}\cdot\mathbf{b}) & \xi & H+cu_n & H-cu_n \\ 0 & 0 & 1 & e_V & e_V \end{bmatrix} \tag{27}$$

where the pressure derivatives are defined as

$$K = \left(\frac{\partial p}{\partial \epsilon_T}\right)_{\rho_q,\epsilon_V} = \frac{\sum_{q'} Y_{q'} R_{q'}}{\sum_{q'} Y_{q'} c^{q'} v_T}$$

$$K_e = \left(\frac{\partial p}{\partial \epsilon_V}\right)_{\rho_q,\epsilon_T} = \frac{Y_e R_e}{\sum_q Y_q c_{vV}^q} \tag{28}$$

$$\chi_{q'} = R_{q'} T - K e_T^{q'} - K_e e_V^{q'}$$

$$\chi_e = \left(1 - \tfrac{3}{2} K_e\right) R_e T_V$$

and

$$c^2 = \sum_q \chi_q Y_q + Kh + (K_e - K) e_V \tag{29}$$

The values at the interfaces are calculated by using a generalization of Roe's averaging[19] to allow for thermal and chemical nonequilibrium.

The numerical viscous fluxes are evaluated by applying Gauss's theorem to a cell whose vertices are the two grid nodes at cell face $(i+\frac{1}{2}, j)$ and the centers of the two adjacent cells (i, j) and $(i+1, j)$, and a bilinear interpolation of cell-center values is employed to determine nodal values.

In the presence of nonequilibrium ionizing flows, stiffness arises for the disparity between the characteristic time scale of the relaxation processes and the fluid-dynamic one. For steady flows the stiffness can be reduced by preconditioning the system of discretized (ordinary differential) equations. The time integration is performed by a three-stage Runge-Kutta algorithm, where the source terms are treated by a point implicit algorithm[6,27] by introducing a precondition matrix that is related to the partial Jacobian of the source term.

Boundary Conditions

At the freestream boundary, depending on the flow direction, either extrapolation conditions or freestream values are imposed. At the outflow, first-order extrapolation is imposed. At the wall, no-slip conditions are enforced on the velocity, zero normal pressure gradient is imposed, and fixed translational wall temperature or adiabatic conditions are set.

It must be pointed out that the use of a two-temperature model may lead to inconsistencies in the wall treatment of the vibrational-electron-electronic energy boundary condition. Indeed, at the wall the flow is generally in thermal equilibrium, i.e., $T_V = T$. However, because of the shielding effect, a wall can also be assumed to be adiabatic with respect to the electron energy flux, i.e., $\partial T_V/\partial n = 0$. At the wall we have then assumed either $T_V = T$ if the vibrational-electronic energy content is greater than the electron translational energy content, or $\partial T_V/\partial n = 0$ otherwise. Gas-surface interaction has been neglected, and Neumann boundary conditions (zero normal gradient) are imposed on the species mass fractions.

Results

In the present work we have analyzed the effects of shock strength on ionization and thermal and chemical nonequilibrium. In particular, we have considered flows characterized by weak shocks (i.e., wedge-type flows) and blunt-body flows characterized by a strong bow shock.

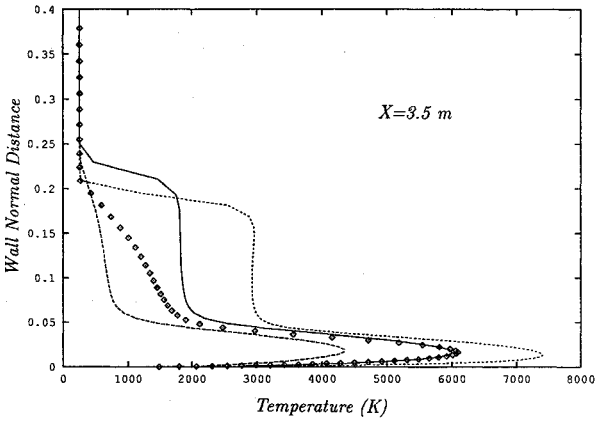

Fig. 1 Wedge (solid curve, T, V_∞ = 8100 m/s; dashed curve, T_V, V_∞ = 8100 m/s; dotted curve, T, V_∞ = 11,000 m/s; diamonds, T_V, V_∞ = 11,000 m/s).

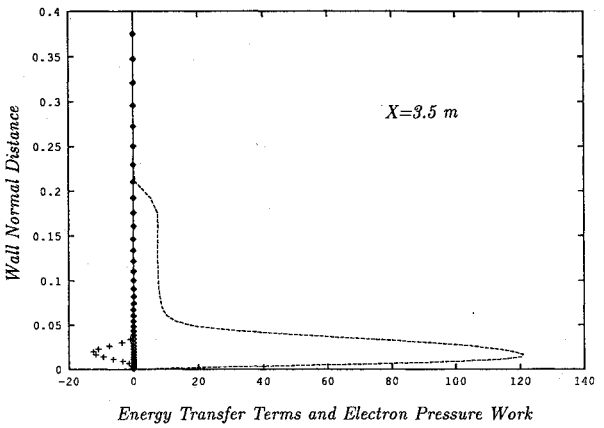

Fig. 2 Wedge, V_∞ = 8100 m/s (solid curve, electron pressure work; dashed curve, T-V energy exchange; diamonds, T-E energy exchange; crosses, energy removal).

Wedge

This test case is rather well defined,[9,28,29] and it has been selected because it allows us to study the interaction effects between the shock (which arises at the apex of the wedge) and the reacting viscous layer. The test case corresponds to the flow over a 10-deg wedge with a length of 4 m, at an altitude of 61 km, a wall temperature of 1200 K, and two freestream velocities: V_∞ = 8100 m/s (this test case is referred to as W1) and V_∞ = 11,000 m/s (referred to as W2). Computations have been performed on two different grids, corresponding to a 176 × 48, and a 176 × 64 mesh, with normal mesh spacing ranging from 1.5 to 70 mm for the first grid, and from 0.14 to 47 mm for the second one.

Figure 1 shows the distributions of the translational and vibrational-electron-electronic temperatures for the two different freestream velocities at 3.5 m from the apex. From the computed results we have found that strengthening the shock (by going from 8100 to 11,000 m/s) is not sufficient to induce enough ionization to alter the temperature distributions. At the lower freestream velocity the inviscid part of the shock layer is nearly frozen, and thermal-nonequilibrium effects occur mainly between the edge of the boundary layer and its core. However, as the temperature increases, all of the shock layer is dominated by thermal-nonequilibrium phenomena. Figure 2 shows the different contributions to the source of vibrational-electron-electronic energy for the test case W1. The figure indicates that translational-vibrational energy transfer and the energy removal due to finite-rate chemistry effects dominate the other terms. Moreover, one also observes that these two contributions have a peak at approximately the same distance from the wall where T and T_V peak, which corresponds to the position where the frictional heating is maximum. The same behavior has been observed for the test case W2.

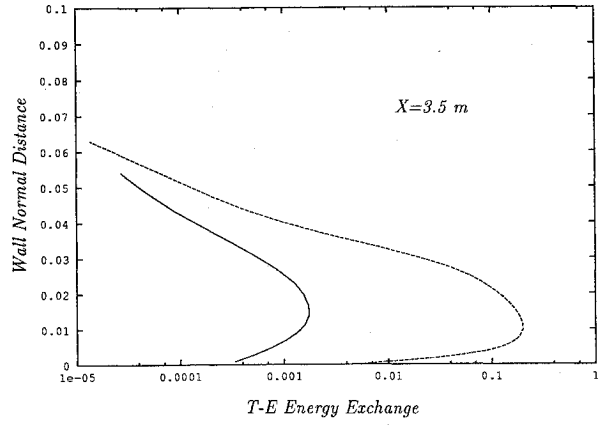

Fig. 3 Wedge (solid curve, T-E, V_∞ = 8100 m/s; dashed curve, T-E, V_∞ = 11,000 m/s).

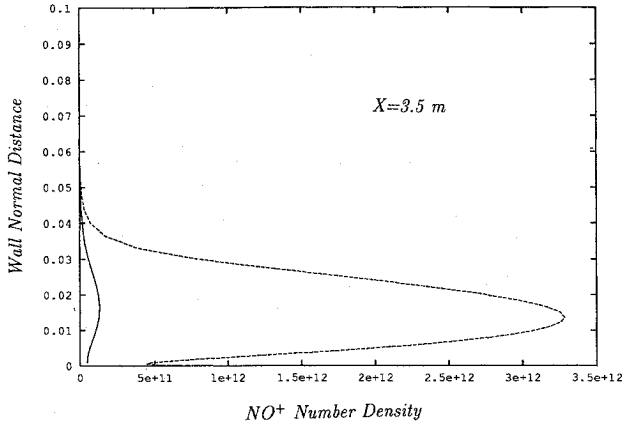

Fig. 4 Wedge (solid curve, V_∞ = 8100 m/s; dashed curve, V_∞ = 11,000 m/s).

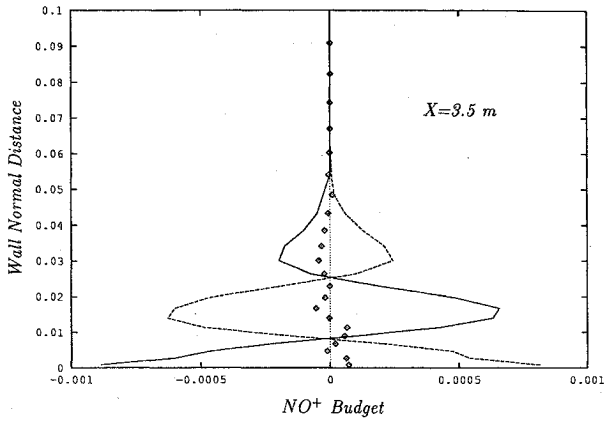

Fig. 5 Wedge V_∞ = 8100 m/s (solid curve, source; dashed curve, diffusion; diamonds, convection).

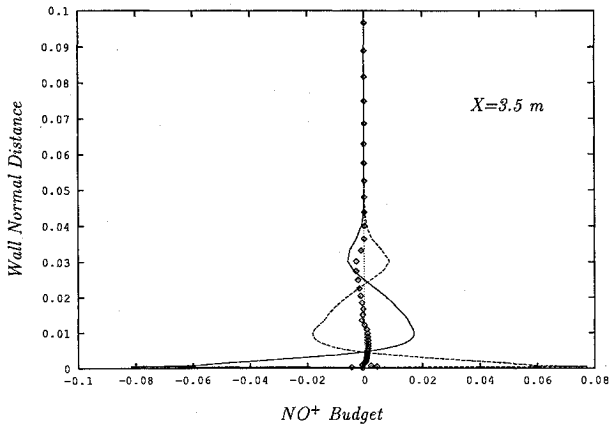

Fig. 6 Wedge V_∞ = 11,000 m/s (solid curve, source; dashed curve, diffusion; diamonds, convection).

The dissipation mechanism is also responsible for the (heavy-particle) translational-electron-electronic energy transfer mechanism, as Figs. 3 and 4 clearly show, where the T-E transfer term and the number density of the nitric oxide ions are reported. The budgets of the nitric oxide ions for the two test cases (W1 and W2) are reported in Figs. 5 and 6, which show that this type of problem is dominated by diffusion and finite-rate processes (note that, under the assumption of zero conduction current, the diffusion velocities of charged particles are equal). Ions are produced in the boundary-layer core due to associative ionization; ionic recombination takes place moving away from the core region, both upward and downward. This is due to the combined effects of the thermal boundary layer and of the diffusion of the charged particles from the core region toward the wall and the edge of the boundary layer. Figure 7 shows a sketch of our interpretation of the ionization mechanism: dominated by diffusion and associative ionization near the peak temperature, and by diffusion and ionic recombination in both the near-wall and boundary-layer edge regions.

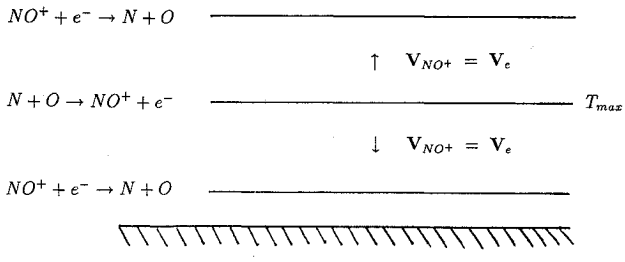

Fig. 7 Schematic of ionization process in a ionizing boundary layer.

RAM-C

This test case corresponds to the flow around a sphere-cone body used for the Radio Attenuation Measurement experiment carried out to assess the effects of blackout during re-entry.[1,2,10] In particular, the cases corresponding to the measurements at 61 and 71 km have been simulated with the objective of identifying the controlling mechanisms.

The geometry is a sphere of 15-cm nose radius with a cone of 9-deg half-angle, having a length of about 130 cm, and flying at a velocity of 7650 m/s at the altitude of 61 km, and of 7645 m/s at 71 km. The computations have been performed for both conditions on a 120 × 64 grid with mesh spacing ranging from 24 μm to 24 mm.

This test case differs substantially from the previous one in that there is a strong bow shock, which is responsible for the large degree of nonequilibrium arising immediately past the shock, as can be observed from Fig. 8. This figure show the computed translational and vibrational temperature distributions along the stagnation line for the two altitudes. Observe that at an altitude of 61 km the nonequilibrium effects are confined to about half of the shock layer. A 10-km increase in altitude reduces the density by a factor of 4. As a consequence the standoff distance increases by approximately 30% and, more importantly, nearly the entire shock layer is in thermal nonequilibrium.

The atomic-oxygen and atomic-nitrogen mass-fraction distributions along the stagnation line are reported in Fig. 9. In both cases (61 and 71 km), the oxygen is fully dissociated. On the other hand, nitrogen is (highly) affected by the altitude (which influences the thermal and chemical relaxation lengths) and shows a much greater degree of dissociation at lower altitudes. Figure 10 shows the comparison of the computed and the measured peak electron number density along the body. The comparison shows very good agreement, with a scatter from the experimental values similar to that reported by other authors.[1,2] From this figure we observe that most of the ionization occurs at stagnation, with a drop in the peak electron number density of two orders of magnitude at a distance of two nose radii from the stagnation point. This is due to the strong expansion of the flow, which causes the freezing of the vibrational-electron-electronic excitation energy, as shown in Fig. 11, where the T and T_V for the 61-km case are reported at $X/R_n = 2$. Indeed,

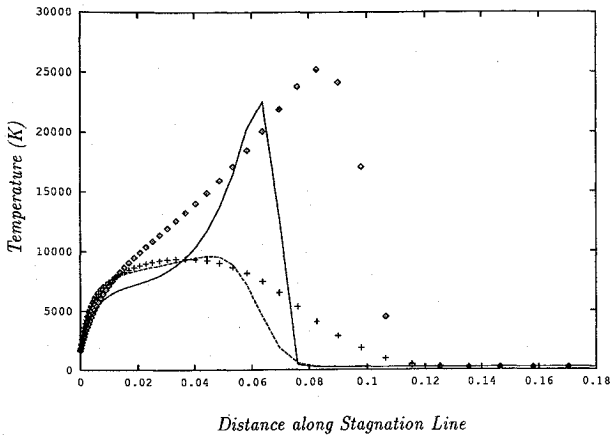

Fig. 8 RAM-C (solid curve, T, 61 km; dashed curve, T_V, 61 km; diamonds, T, 71 km; crosses, T_V , 71 km).

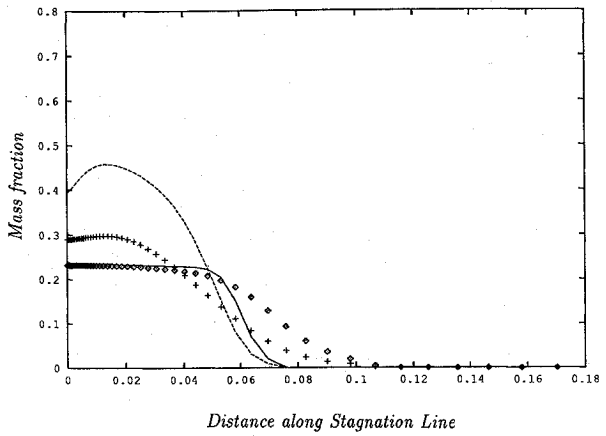

Fig. 9 RAM-C (solid curve, O , 61 km; dashed curve, N, 61 km; diamonds, O, 71 km; crosses, N, 71 km).

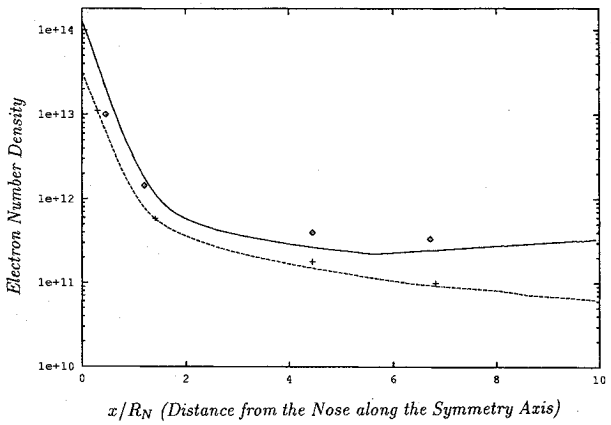

Fig. 10 RAM-C (solid curve, 61 km computed; dashed curve, 71 km computed; diamonds, 61 km measured; crosses, 71 km measured).

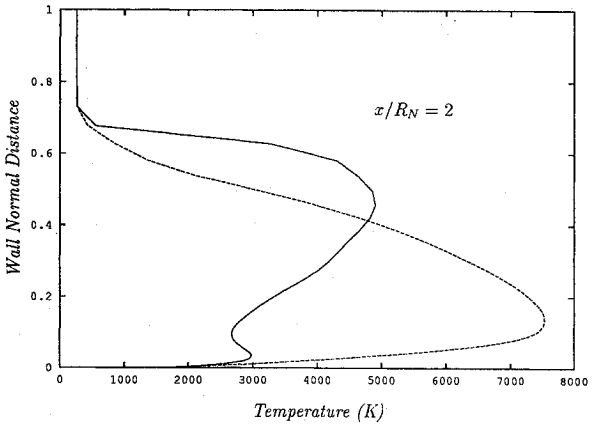

Fig. 11 RAM-C, 61 km (solid curve, T; dashed curve, T_V).

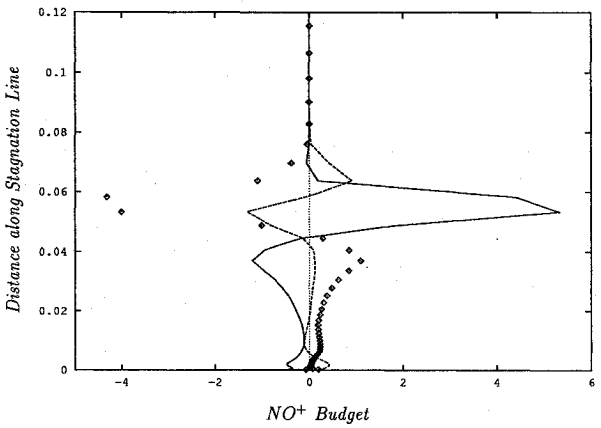

Fig. 12 RAM-C, 61 km (solid curve, source; dashed curve, diffusion; diamonds, convection).

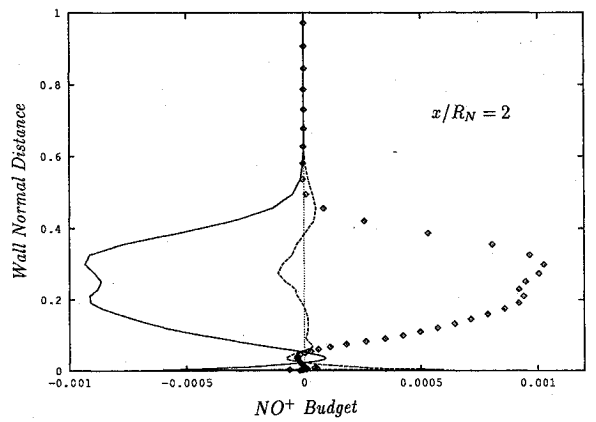

Fig. 13 RAM-C, 61 km (solid curve, source; dashed curve, diffusion; diamonds, convection).

comparing the peak values of T and T_V, one observes a drop in T by a factor of about 5 (measured as the ratio of the peak value at stagnation to the corresponding one at $X/R_n = 2$), and a drop in T_V by a factor of about 1.3. Note that for the 61-km case we predict a slight increase of the peak electron number density at $X/R_n > 5$, which is probably due to the use of a two-temperature model. Indeed, this increase is also observed in the (two-temperature) computations by Palmer,[2] whereas it is not noticeable in the results obtained with a six-temperature model.[1]

The budgets of the nitric oxide ions at stagnation and $X/R_n = 2$ are reported in Figs. 12 and 13. These figures clearly show the inviscid ionization mechanism (except in the near vicinity of the stagnation region) typical of blunt-body flows at intermediate altitudes: the shock layer is dominated by convection and heavy-particle dissociation and ionization reactions, and the diffusion is negligible almost throughout, except in the very near-wall region. Associative ionization around stagnation is responsible for the formation of charged particles, which are then convected away and recombine (by ionic recombination) because of the flow expansion.

To assess the influence of the grid on the solution, three additional computations for the 61-km test case have been carried out on 60 × 32 ($\Delta y_{\min} = 53$ μm), 60 × 64 ($\Delta y_{\min} = 24$ μm), and 60 × 128 ($\Delta y_{\min} = 12$ μm) meshes. The computed results are reported in Figs. 14 and 15, which show the translational temperature along the stagnation line and the electron peak number density along the body. The figures show that the discretization in the normal direction affects primarily the peak temperature value and the shock thickness. If the number of cells in the normal direction is doubled, a 10% variation in the peak temperature value due to a greater resolution of the bow shock is obtained, and the latter is not affected by the number of grid cells along the body. Defining the standoff distance

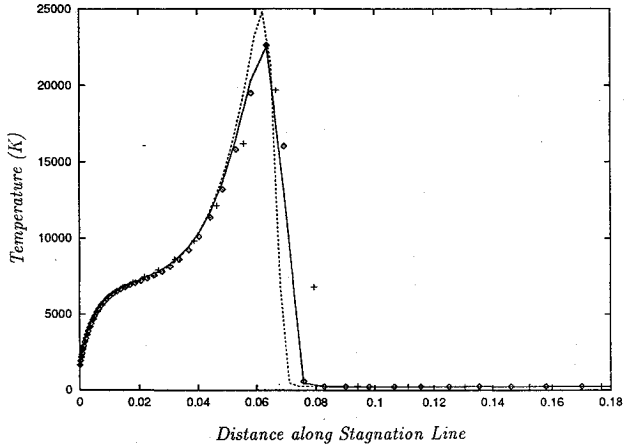

Fig. 14 Grid sensitivity for RAM-C, 61 km (solid curve, 120 × 64; diamonds, 60 × 64; dashed curve, 60 × 128; crosses, 60 × 32).

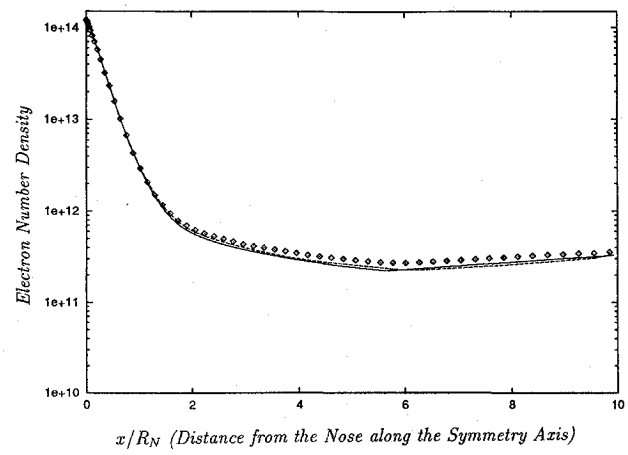

Fig. 15 Grid sensitivity for RAM-C, 61 km (solid curve, 120 × 64; dashed curve, 60 × 64; diamonds, 60 × 32).

as the distance along the stagnation line at which the density ratio is equal to 6, we also observe that the displacement of the shock (with respect to the 120 × 64 grid) is at most 6% for the coarsest grid, and 0.6% for the 60 × 128 grid. However, the differences in the peak temperature do not affect the ionization, as shown in Fig. 15, this is to be expected, as the problem is dominated by convection and ionization.

Conclusions

The effects of the shock strength on ionization and thermochemical nonequilibrium have been studied. In the presence of a weak oblique shock it is found that viscous dissipation is responsible for activating finite-rate processes. Moreover, an ionizing boundary layer is characterized by three layers: a core region dominated by diffusion and associative ionization, an inner (near the wall) layer, and an outer (near the boundary-layer edge) region dominated by diffusion and ionic recombination. In the presence of a strong bow shock the ionization is found to be mainly an inviscid phenomenon. Charged particles formed by associative ionization reactions occurring in the strong shocked region (stagnation), are convected away from the stagnation zone and recombine (by ionic recombination) because of flow expansion. As a consequence, if the main objective is the prediction of the blackout, a rather coarse grid can be employed, even though the shock resolution will be poor.

References

[1]Deiwert, G. S., and Candler, G. V., "Three-Dimensional Supersonic and Hypersonic Flows Including Separation," AGARD Report 764, May 1989.

[2]Palmer, G., "The Development of an Explicit Thermochemical Nonequilibrium Algorithm and Its Applications to Compute Three Dimensional AFE Flowfields," AIAA Paper 89-1701, June 1989.

[3]Hatfield, J. A., and Candler, G. V., "Examination of Nonequilibrium Effects in an Ionized Nitrogen Flow," AIAA Paper 93-0478, Jan. 1993.

[4]Mitcheltree, R. A., "A Parametric Study of Dissociation and Ionization Models at 12 km/sec," AIAA Paper 91-1368, June 1991.

[5]Gnoffo, P. A., Gupta, R. N., and Shinn, J. L., "Conservation Equations and Physical Models for Hypersonic Air Flows in Thermal and Chemical Nonequilibrium," NASA TP 2867, Feb. 1989.

[6]Grasso, F., and Bellucci, V., "Thermal and Chemical Nonequilibrium Hypersonic Flow Computations," AGARD-70 FDP, Paper 43, May 1992.

[7]Shebalin, J. V., "Aerobrake Plasmadynamics: Macroscopic Effects," *Journal of Spacecraft and Rockets*, Vol. 28, No. 4, 1991, pp. 394–400.

[8]Vincenti, W. G., and Kruger, C. H., Jr., *Introduction to Physical Gas Dynamics*, Wiley, New York, 1965.

[9]Grasso, F., and Bellucci, V., "Modeling of Hypersonic Nonequilibrium Flows," *Advances in Hypersonics: Modeling Hypersonic Flows*, edited by J. Bertin, J. Periaux, and J. Ballmann, Vol. 2, Birkhäuser, Boston, 1992, pp. 128–175.

[10]Park, C., *Nonequilibrium Hypersonic Aerothermodynamics*, Wiley, New York, 1990.

[11]Park, C., and Yoon, S., "Calculation of Real-Gas Effects on Blunt-Body Trim Angles," AIAA Paper 89-0685, Jan. 1989.

[12]Gupta, R. N., Yos, J. M., Thompson, R. A., and Lee, K. P., "A Review of Reaction Rates and Thermodynamic and Transport Properties for an 11-Species Air Model for Chemical and Thermal Nonequilibrium Calculations to 30 000 K," NASA RP 1232, Aug. 1990.

[13]Lee, J. H., "Basic Governing Equations for the Flight Regimes of Aeroassisted Orbital Transfer Vehicles," *Thermal Design of Aeroassisted Orbital Transfer Vehicles*, edited by H. F. Nelson, Vol. 96, Progress in Astronautics and Aeronautics, AIAA, New York, 1985, pp. 3–53.

[14]Park, C., "Convergence of Computation of Chemical Reacting Flows," AIAA Paper 85-0247, Jan. 1985.

[15]Hansen, C. F., "Collision-Induced Gas Phase Dissociation Rates," NASA NAG 1-1046, Aug. 1990.

[16]Park, C., "Assessment of Two-Temperature Kinetic Model for Ionizing Air," AIAA Paper 87-1574, June. 1987.

[17]Millikan, R. C., and White, D. R., "Systematics of Vibrational Relaxation," *Journal of Chemical Physics*, Vol. 39, No. 12, 1963, pp. 3209–3213.

[18]Appleton, J. P., and Bray, K. N. C., "The Conservation Equations for a Nonequilibrium Plasma," *Journal of Fluid Mechanics*, Vol. 20, No. 4, 1964, pp. 659–672.

[19]Roe, P. L., "Approximate Riemann Solvers, Parameter Vectors, and Difference Schemes," *Journal of Computational Physics*, Vol. 43, No. 2, 1981, pp. 357–372.

[20]Steger, J. L., and Warming, R. F., "Flux Vector Splitting of Inviscid Gasdynamics with Application to Finite Difference Methods," *Journal of Computational Physics*, Vol. 40, No. 2, 1981, pp. 263–293.

[21]Van Leer, B., "Flux-Vector Splitting for the Euler Equations," Institute for Computer Applications in Science and Engineering, Report 82-30, Sept. 1982.

[22]Glaister, P., "An Approximate Linearized Riemann Solver for the Three Dimensional Euler Equations for Real Gases Using Operator Splitting," *Journal of Computational Physics*, Vol. 77, No. 2, 1988, pp. 361–383.

[23]Liou, M. S., Van Leer, B., and Shuen, J. S., "Splitting of Inviscid Fluxes for Real Gases," *Journal of Computational Physics*, Vol. 87, No. 1, 1990, pp. 1–24.

[24]Grossman, B., Cinnella, P., and Garrett, J., "A Survey of Upwind Methods for Flows with Equilibrium and Non-Equilibrium Chemistry and Thermodynamics," AIAA Paper 89-1653, June 1989.

[25]Montagné, J. L., Yee, H. C., Klopfer, G. H., and Vinokur, M., "Hypersonic Blunt Body Computations Including Real Gas Effects," NASA TM-100074, Mar. 1988.

[26]Liu, Y., and Vinokur, M., "Upwind Algorithms for General Thermo-Chemical Nonequilibrium Flows," AIAA Paper 89-0201, Jan. 1989.

[27]Bussing, T. R. A., and Murman, E. M., "Finite-Volume Method for the Calculation of Compressible Chemically Reacting Flows," AIAA Paper 85-0331, Jan. 1985.

[28]Prabhu, D. K., Tannehill, J. C., and Marvin, J. G., "A New PNS Code for Chemical Nonequilibrium Flows," *AIAA Journal*, Vol. 26, No. 7, 1988, pp. 808–815.

[29]Candler, G., "On the Computation of Shock Shapes in Nonequilibrium Hypersonic Flows," AIAA Paper 89-0312, Jan. 1989.

I. D. Boyd
Associate Editor